Journal of Power Sources 641 (2025) 236824

Contents lists available at ScienceDirect

Journal of Power Sources

journal homepage: www.elsevier.com/locate/jpowsour

Development of biomass pyrolysis bio-oil as a renewable surface engineering agent for bio-based hard carbon production

Yanghao Jin [a,1], Huiting Liu [b,c,1], Hanmin Yang [a], Dumindu Pasan Siriwardena Thanaweera Achchige [d], Yaprak Subasi [d], Ritambhara Gond [d], Yazhe Wang [a], Habtom Desta Asfaw [d], Shiwei Chen [e], Ziyi Shi [a,*], Tong Han [a,**], Manuel Baumann [b], Niklas von der Assen [c], Marcel Weil [b,f], Reza Younesi [c], Pär G. Jönsson [a], Weihong Yang [a]

[a] Department of Material Science and Engineering, KTH Royal Institute of Technology, Stockholm, 114 28, Sweden
[b] Institute for Technology Assessment and Systems Analysis, Karlsruhe Institute of Technology, Karlstr. 11, 76133, Karlsruhe, Germany
[c] Institute of Technical Thermodynamics, RWTH Aachen University, Schinkelstr. 8, 52062, Aachen, Germany
[d] Department of Chemistry - Ångström Laboratory, Uppsala University, Lägerhyddsvägen 1, Box 538, Uppsala, 75121, Sweden
[e] University of Michigan-Shanghai Jiao Tong University Joint Institute, Shanghai Jiao Tong University, Shanghai, 200240, PR China
[f] Helmholtz Institute Ulm, Helmholtzstr. 11, 89081, Ulm, Germany

HIGHLIGHTS

- A novel bio-oil blended hard carbon synthesis approach has been developed.
- Bio-oil has potential as a sustainable surface engineering agent.
- The yield of the bio-oil blended hard carbon (BHC) was increased by 40 %.
- BHC performed higher initial coulombic efficiency, reaching 89.9 %.
- BHC reduced its greenhouse gas emissions by 20 % in life cycle assessment.

GRAPHICAL ABSTRACT

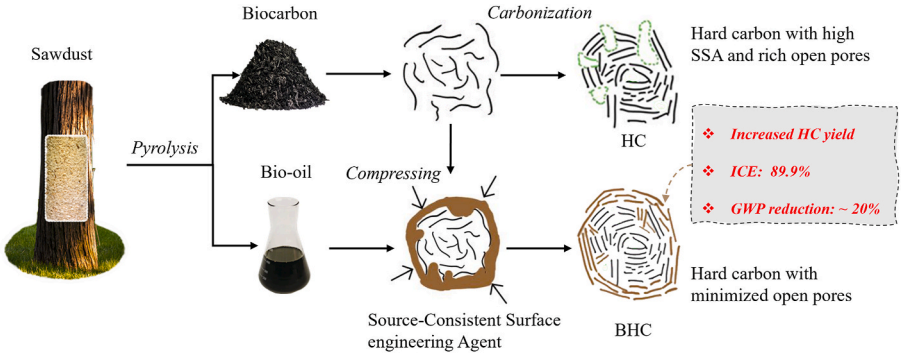

ABSTRACT

Sodium-ion batteries (SIBs) are emerging as a promising alternative to lithium-ion batteries due to their potential for efficient and sustainable energy storage. Thus, the demand for high-performance battery materials with a sustainable supply chain, particularly hard carbon (HC) as the primary anode material for SIBs, is rapidly increasing. This study focuses on enhancing the production and electrochemical performance of HC products by leveraging Sweden's abundant forestry resources and advanced biomass refining processes. Specifically, we propose a novel HC production process that compresses sawdust-derived biocarbon with bio-oil derived from the same pyrolysis process to produce HC with improved properties, where the bio-oil serves as both a binder and a surface engineering agent for the biocarbon. This approach effectively modifies surface defects, leading to increased initial Coulombic efficiency (ICE), reaching values of 90 % in half-cell tests. Moreover, laboratory

* Corresponding author.
** Corresponding author.
E-mail addresses: ziyis@kth.se (Z. Shi), tong.han@nordicbiographite.com, tongh@kth.se (T. Han).
[1] Yanghao Jin and Huiting Liu contributed equally to this work.

https://doi.org/10.1016/j.jpowsour.2025.236824
Received 2 April 2024; Received in revised form 9 March 2025; Accepted 16 March 2025
Available online 23 March 2025

measurements and Life Cycle Assessment (LCA) results quantified that this production method achieves nearly 50 % higher HC yields and reduces greenhouse gas (GHG) emissions by approximately 20 % compared to the conventional production method. As a result, this offers a potentially more sustainable and economically viable solution for advancing the SIB anode material production.

1. Introduction

Sodium-ion batteries (SIBs) are garnering significant attention as a viable alternative to lithium-ion batteries (LIBs), due to their use of more abundant raw materials and potential for cost reduction [1]. Projections indicate that the global market for SIBs is expected to escalate to approximately 4368 million USD by 2030 [2], underscoring the urgent need for sustainable battery materials to meet the rapidly increasing demand for SIBs.

Hard carbon (HC) is currently the primary anode material used in SIB prototypes due to its cost-effectiveness, electrochemical stability, and promising sustainability potential [3,4]. HC is typically produced through the carbonization of thermosetting precursors such as anthracite [5], phenolic resin [6], and various forms of biomass [7]. Biomass waste is particularly promising among these precursors due to its availability, sustainability, and potential electrochemical performance [8]. However, as shown in Table 1 [9–18], HC is still in the early stages of development compared to graphite (the most commonly used anode material in LIBs).

One of the key challenges is the electrochemical performance of bio-based HC products, particularly their low initial Coulombic efficiency (ICE). The ICE of bio-based HC is typically below 80 % (Fig. S1), posing a significant barrier to its commercial application in SIBs, which generally require an ICE above 85 % [19]. This phenomenon can be ascribed to the retention of the intrinsic surface structure of the biomass after carbonization [20], characterized by the extensive presence of surface defects, porosity, and specific surface area (SSA), all of which contribute to the formation of irreversible solid electrolyte interphase (SEI) layer [21]. Therefore, specific surface engineering methods to improve the ICE of biomass-based HC are essential for large-scale commercialization [22].

Among them, one notable method of surface engineering — creating additional carbon layer on the surface and within the open pores of HC — is currently being implemented [23,24]. This method can effectively reduce SSA and defect sites, thereby boosting the ICE and also enhancing cycling stability [25]. For instance, Zhang et al. used polypropylene (PP) chemical deposition to form a carbon layer on the exterior of asphalt-based HC, which effectively reduced the SSA from 317.7 to 26.2 m^2/g, and increased ICE values from 38.6 % to 81.1 % [26]. Chen et al. employed space-confined chemical vapor deposition (SC-CVD) to fill activated carbon with benzene vapor. This method dramatically reduced the specific surface area from 1623 to 74 m^2/g and increased the ICE from 22.7 % to 81.9 % [27]. However, these methods typically rely on extra fossil fuel–derived agents (Table S1), which not only increase production complexity and cost but may also result in a more significant environmental burden. These factors conflict with the growing emphasis on sustainable and circular battery manufacturing practices, as exemplified by recent EU Green Battery policies [28]. Therefore, a novel sustainable surface engineering approach is still worthy of investigation.

Bio-oil, a byproduct from biocarbon (precursor of bio-based HC) production, offers a renewable alternative as a surface engineering agent. On the one hand, bio-oil has a high carbon content and natural affinity for biocarbon, which enables it to coat biocarbon surfaces and infiltrate their open pores through a simple blending and compression process. Upon carbonization, bio-oil will form coke [29], creating extra carbon layers on the surface and within the open pores, thereby reducing the SSA of HC and increasing the ICE. Moreover, bio-oil is derived from the same biomass precursor as HC, and the properties of the extra carbon layer would be the same as those of carbons in HC, which would not affect the overall homogeneity of HC. On the other hand, as a by-product that accounts for over 50 % of the total yield, bio-oil is abundant, inexpensive, and easy to obtained [30]. Reusing bio-oil can significantly enhance production efficiency by increasing the overall yield of HC [31], thereby contributing to a potinitially more sustainable manufacturing process.

Herein, capitalizing on the abundant forestry resources and mature biomass refining processes in Sweden, we propose a high-yield and sustainable production method for sawdust-derived HC. Specifically, this process utilizes sawdust-derived biocarbon and bio-oil as the precursor. Through a process of mixing, compressing, and carbonizing, the SSA and defects of sawdust-derived HC are reduced, resulting in HC products with improved ICE values, higher yields, and a lower carbon footprint.

2. Material and method

2.1. Materials

Raw biocarbon powder and bio-oil, provided by Envigas AB, were used as precursors for producing HC. The biocarbon powder and bio-oil were obtained from the pyrolysis of sawdust at 550 °C using a bubbling fluidized bed system. The results of the proximate analysis and elemental analysis of the biocarbon are presented in Table S2 and Table S3 supplemental information.

2.2. Experiment procedure

The experiment procedure is shown in Fig. 1. The raw biocarbon powder and bio-oil were provided by a biomass refinery. The biocarbon was ground into particles with a size smaller than 32 μm. The resulting biocarbon was mixed with the bio-oil in an 70:30 ratio. The mixture was then heated at 100 °C for 5 min in a drying oven to soften the bio-oil and to ensure a thorough mixing. As shown in Fig. S2, the mixture was

Table 1
Comparation of the Hard Carbon (for SIB) and Synthetic Graphite (for LIB) anode materials.

	Raw material	Temperature	Heating method	Yield from raw material	Production line size	Price	Carbon footprint	Amount in battery	Cost ratio	ICE	Ref.
		°C		%	t/year	USD/kg	kg CO2/kg	t/GWh	%	%	
Hard Carbon (SIB)	Phenolic Resin, Biomass, Petroleum pitch	1200–1400	Resistance heating	15 %–55 %	400–2000	3–300	Depend on raw material	1600	15~25 %	>80 %	[9–15]
Synthetic Graphite (LIB)	Coal	2500–3000	Resistance heating, Joule heating	85 %–90 %	>10000	0.4–10	5.5–13.8	1000	5~12 %	>95 %	[12, 15–18]

pressed into carbon columns with diameters of 10–40 mm using a mold under 10-bar pressure and named by Precursor of bio-oil mixed hard carbon (Pre-BHC). The Pre-BHCs were first devolatilization at 800 °C then heated to 800, 1000, and 1300 °C for 3 h under an N_2 atmosphere at a heating rate of 20 °C/min. The resulting bio-oil mixed hard carbon (BHC) blocks were ground into particles with a diameter smaller than 32 μm and labeled as BHC-800, BHC-1000, and BHC-1300 based on the carbonization temperature. For the reference process, the biocarbon was first heated to 800 °C at a rate of 5 °C/min under an N_2 atmosphere and held for 3 h to remove volatile components. It was then carbonized at 800 °C, 1000 °C, and 1300 °C at a rate of 20 °C/min for 3 h under an N_2 atmosphere. The resulting HC products are referred to as HC-800, HC-1000, and HC-1300, respectively.

2.3. Characterization method

The ultimate composition and proximate analyses, including the moisture, fixed carbon, volatile, and ash contents of the raw biomass, were conducted by Eurofins Biofuel & Energy Testing Sweden AB.

A scanning electron microscope (SEM) (The JEOL JSM-7800F, JEOL Ltd., Akishima, Japan, and Ultra 55 ZEISS) was used to study the detailed morphologies of HC. Each sample was fixed on a steel sample holder using carbon tape. An acceleration voltage of 10 kV and a working distance of 8–10 mm were used to take images.

Powder X-ray diffraction (XRD) patterns of the samples were obtained using a Bruker D8 Advance diffractometer with Cu Kα X-ray radiation (λ = 0.15418 nm). The instrument was operated by scanning the Bragg angle (2θ) from 10° to 80° with a step size of 0.02°. The interlayer spacing (d_{002}) of each sample was calculated from the Bragg angle of the diffraction peak for the (002) plane in the XRD spectra using Bragg's equation [32]:

$$d_{002} = \frac{\lambda}{2\ sin\ \theta}.$$

The stacking height (L_c-002 plane) and the crystallite size (L_a-100 plane) of each sample are calculated using the following equation [33]:

$$L_a = \frac{k_1\lambda}{\beta_{(100)}cos\theta} \quad L_c = \frac{k_2\lambda}{\beta_{(002)}\ cos\ \theta}$$

where k is the Scherrer parameter (k_1 = 1.84, k_2 = 0.94), β represents the full width at half the maximum (FWHM) of the diffraction peak. The parameter θ stands for the Bragg angle corresponding to the diffraction peak.

Evaluation of the porosity and the Brunnauer-Emmet-Teller (BET) specific surface areas of the HC samples was conducted using N_2-gas physisorption at 77.36 K using ASAP2020 analyzer (Micromeritics®). The samples (~0.4–0.6 g powder) were degassed at 90 °C for about 1 h and at 400 °C for 6 h prior to gas adsorption/desorption analysis.

The Raman spectrum of HC nanosheets was collected using a Tyrode I Raman microscope equipped with a 532-nm wavelength diode laser at a power of 5 MW. The Raman spectra was obtained at the laser power of 50 MW with the expose time of 1min.

The sample of the BHC-1300 powder was dispersed in ethanol and sonicated in preparation for Transmission Electron Microscopy (TEM) analysis. A drop of the dispersion was placed on the TEM grid and dried. TEM analysis was conducted on JEOL® JEM-2100F at 200 kV with Gatan CCD camera. The selected-area electron diffraction (SAED) and TEM images were recorded by a Gatan® Orius 200D and Ultrascan 1000 XP camera, respectively.

True density data were recorded on an AccuPyc II 1340 analyzer using Helium as analysis gas. Using the ideal graphite density of 2.26 g/cm^3 as a baseline, the volume of the closed pores in HC can be obtained [34].

2.4. Electrochemical test

The electrochemical sodium (de)intercalation properties in BHC samples are examined using pouch cells (half-cells). The carbon anodes were prepared by mixing the active material and CMC (sodium salt of carboxymethyl cellulose, Sigma-Aldrich-average M_w~700,000) binder with a mass ratio of 95:5 in deionized water (~1.80 ml for 0.5 g of material mixture) and casting the slurry on a C-coated Al foil (using 350 μm doctor blade), followed by a drying process at 120 °C overnight in a Buchi oven inside the Glove box. The mass loading of the active material is approximately controlled between 3 and 5 mg cm^{-2}. Battery cells were made using HC as the working (13 mm) and Na metal (15 mm) as the counter electrodes. These were separated by a 20 mm GF/A separator soaked with 120 μL of 1 M $NaPF_6$/Diglyme electrolyte. The electrochemical performance is evaluated by galvanostatically charging and discharging the cell using a LANDT CT2001 battery tester in the voltage range of 0.001–2.5 V at 20 mA/g, in CC mode, at room temperature (25 °C). CV measurements at multiple rates for BHC1300 material were obtained using a Biologic VMP2 potentiostat. The scan rates used were 0.1, 0.2, 0.4, 1.0 and 2.0 mV/s.

2.5. Life cycle assessment

Potential environmental impacts from producing sawdust-derived HC materials are analyzed by applying a cradle-to-gate Life Cycle Assessment (LCA) for two scenarios, i.e. two different synthesis routes as shown in Fig. 1.

- Scenario 1: HC-1300 (conventional biocarbon powder at 1300 °C pyrolysis temperature) with synthesis route 1
- Scenario 2: BHC-1300 (compressed column with bio-oil at 1300 °C pyrolysis temperature) with synthesis route 2.

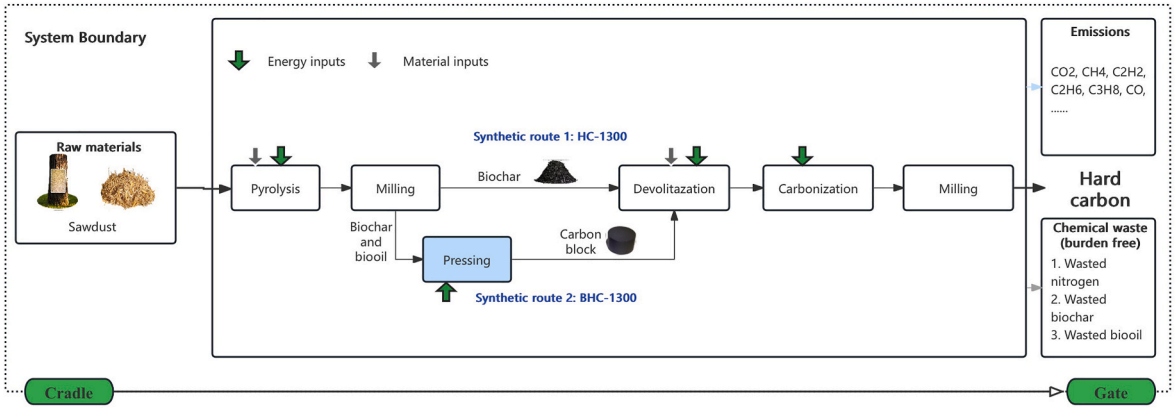

Fig. 1. Laboratory production process of HC including the considered cradle-to-gate system boundary.

The flow diagram of both process pathways and system boundary can be found in Fig. 1. For the modelling, 1 kg HC has been chosen as the functional unit. The widely used and accepted life cycle impact assessment method ReCiPe 2016 midpoint (H) is used to provide 18 different impact indicators for the two scenarios. The table of input and output inventories for the two scenarios are included in the Supporting Information (see Tables S3–4).

The most relevant impact indicators, "acidification potential (AP)" (terrestrial acidification), "global warming potential (GWP)", "resource depletion potential (RDP)" (fossil resource scarcity), "water resource depletion (WRP)" and "particulate matter (PM)" (fine particulate matter formation) are chosen according to the product environmental footprint category rules (PEFCR) for rechargeable batteries from the European Commission [35]. Additionally, "human toxicity (HT)" (representative of human carcinogenic toxicity) is also included as the result reflects a significant difference in the two scenarios and often discussed in battery LCA studies [36].

The modeling of the foreground system is based on primary data that are directly measured in the laboratory during the HC synthesis, covering the energy consumption as well as the material inputs and outputs. The energy consumption is associated with the maximum capacity of the corresponding production devices. The background system for the supply chain of materials and energy is modeled from the commercial database Ecoinvent v3.8. The base-case scenario uses the supply chain and electricity mix in Sweden. To investigate the sensitivity against alternative background systems and to explore optimization scenarios for improving the sustainability of HC production, more scenarios are considered as followed: 1. Chinese supply chain and electricity mix; 2. German supply chain and electricity mix. In addition, consideration has also been given to the future clean energy utilization scenarios, where energy is supplied entirely through wind and solar power, and renewable E-mix with 50 % wind and 50 % solar power. Furthermore, the sawdust precursor is considered as biowaste from forest industry. Therefore, the supply chain of the precursors is free of environmental burden. All the environmental impacts caused by the production process are allocated to the main product HC. The analysis is performed by using openLCA V1.11 software.

3. Results and discussion

3.1. Characterization of HC and BHC samples

The morphology of the BHC samples is examined using SEM and TEM. As shown in Fig. S3, after pyrolysis, the biocarbon retains the structural characteristics inherent to its precursor, displaying a wrinkled surface and an internal porous channel structure, with particle sizes predominantly in the 1–2 mm range. Following the milling process, as illustrated in Fig. S4, the particle size of the biocarbon is significantly reduced to values less than 20 μm, with the biocarbon predominantly presenting as thin flakes. It is noteworthy that a small fraction of the particles retain micrometer-scale channels. Although bio-oil is a non-conductive material that may not be distinctly visible in SEM images, higher magnification reveals that the incorporation of bio-oil results in the irregular agglomeration of biocarbon particles. It indicates that the biocarbon surfaces are successfully coated with bio-oil, as depicted in Fig. S5. The compression of this mixture under pressure forms a block-shaped product (Pre-BHC), as demonstrated in Fig. S2.

Fig. 2 displays SEM images of the surface morphology of the Pre-BHC and the BHC-1300 after heat treatment. The SEM image of the Pre-BHC, as shown in Fig. 2a, demonstrates that the biocarbon particles are agglomerated due to the combined effects of pressure and bio-oil. At higher magnification (Fig. 2b), the surfaces of the carbon particles display wrinkled textures adorned with numerous nanometer-sized particles, which are believed to be a result of the bio-oil coating of the wrinkled surfaces. Fig. 2c presents an SEM image of the BHC following the devolatilization and carbonization process. This image clearly shows that the spacing between individual carbon particles is maintained. This observation suggests that the bio-oil present in the interparticle gaps on the surface is removed during the devolatilization process and did not form additional biocarbon between carbon particles. At higher magnifications (Fig. 2d), it is evident that the particles maintain their pre-compression shape, but the surfaces of the HC particles are significantly smoother compared to Pre-BHC. This change implies that the bio-oil, which infiltrated the surface of the biocarbon, altered the wrinkled structure of the biocarbon during the high-temperature process.

TEM and SAED are employed to conduct a more detailed

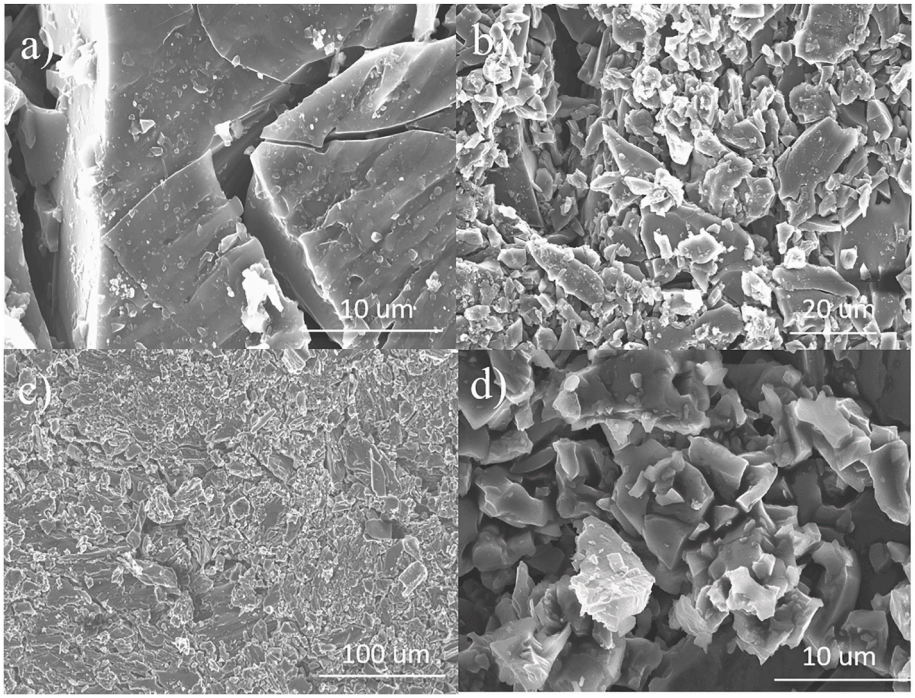

Fig. 2. SEM images of a) and b) Pre-BHC, c) and d) BHC-1300 sample in block shape.

investigation of the carbon microstructure. The TEM microscopy images of the milled BHC-1300 are shown in Fig. 3a and b. As anticipated for HCs, a disordered structure is observed, further confirming the amorphous nature of BHC. The SAED patterns display dispersed diffraction rings, providing additional evidence of the HC structure [37]. Moreover, graphitic domains and nanopores framed by graphene sheets are visible. Notably, the BHC samples display a continuous ordered graphitic layer on their surface due to the carbonization of bio-oil, which coating on the biocarbon particles. These curved graphitic layers also formed closed pores with diameters ranging from 5 to 20 nm. This observation aligns with the smoother surface appearance of BHC particles as seen in the SEM image (Fig. 2d), further explicating the bio-oil surface modification effects on HC during the carbonization process.

To further characterize the microstructure of BHC samples, XRD and Raman spectroscopy are utilized, with the findings presented in Fig. 4a and b. The XRD patterns of all samples reveal broad peaks at 24° and 43°, which are associated with the (002) and (100) crystallographic planes of disordered carbon structures [38]. The average interlayer spacing of graphene sheets (d_{002}), along with the average lateral size (L_a) and thickness (L_c) of graphitic crystallites, are estimated from the XRD data and are listed in Table 2. As the carbonization temperature increases, the d_{002} value of the BHC samples decreases from 0.376 to 0.363 nm, while for the HC samples, it decreases from 0.38 to 0.371 nm. Simultaneously, the L_c of the BHC samples increases from 0.95 to 1.24 nm, and for the HC samples, it increases from 0.89 to 1.07 nm. This indicates that the graphitic-like domains within the HC structure expand with rising carbonization temperatures, resulting in a more ordered structure [39]. Moreover, at the same carbonization temperature, the BHC samples exhibit a lower d_{002} value and a higher L_c value, suggesting that the blending and compressing method using bio-oil influences the internal crystal structure of the HC, promoting a more ordered structure and increasing the graphitization degree of HC.

The Raman spectra, as shown in Fig. 4, display two distinct characteristic bands: the D-band (the defect-induced band) peak at around 1343 cm^{-1} and the G-band (the crystalline graphite band) peak at around 1589 cm^{-1}, confirming the amorphous structure of HC [40]. The intensity ratio of the D and G bands is calculated to compare the defect density [41]. In the prepared HC samples, the I_D/I_G ratio decreases significantly with increasing temperature, indicating that higher temperatures promote graphitization and reduce the defect sites in HC. When comparing HC and BHC samples, it is evident that at the same carbonization temperature, BHC exhibits a lower I_D/I_G ratio. Specifically, HC-1300 has a ratio of 1.86, while BHC-1300 is at 1.59; similarly, HC-1000 has a ratio of 2.08, whereas BHC-1000 is at 1.64. This reduction in the I_D/I_G ratio for BHC can be attributed to the surface engineering effect of bio-oil, which reduces the defect sites on the surface of HC. However, at 800 °C, there is no significant difference in the I_D/I_G ratio, suggesting that bio-oil surface engineering requires a higher carbonization temperature to be effective. The 2D band at 2700 cm^{-1} is used to evaluate the number of stacked graphene layers [4]. Compared to HC samples, BHC samples have a more characteristic 2D peak, indicating the formation of long-range of ordering stacked carbon layers from bio-oil [42,43]. Furthermore, the I_{2D}/I_G ratio of BHCs increases with the rising temperature, suggesting that higher temperatures promote stacked carbon layer formation.

To elucidate the variations in the specific surface area (SSA) of the produced samples, nitrogen adsorption-desorption measurements are conducted. The data reveal that the SSA of BHC samples dramatically decreases from 330 m^2/g to 9 m^2/g, while for HC samples, it decreases from 348 m^2/g to 28 m^2/g as the carbonization temperature increases from 800 °C to 1300 °C. This significant reduction suggests that higher carbonization temperatures contribute to a decreased surface area. Notably, at the same carbonization temperature, BHC samples always exhibit much lower SSA compared to HC samples. This indicates that the addition of the bio-oil and the subsequent high-pressure compressing process is beneficial for reducing open pore.

A true density test using He gas is conducted to further develop the surface engineering effect of bio-oil. Since He can penetrate almost all open pores except for closed ones, closed pore volume of the HC products deduced by comparing their densities to the ideal graphite density (2.26 g/cm^3) [44], which represents pure carbon without open or closed pores. BHC-1300 sample (1.95 g/cm^3) shows a lower true density than HC-1300 (2.00 g/cm^3), which corresponds to the close pore volume increased by nearly 23 % from 0.057 to 0.070 cm^3/g after bio-oil surfaced engineering. This indicates that the bio-oil has filled the open pores on the surface of the HC, converting them into closed pores after carbonization.

The storage density of the BHC samples is determined by measuring their weight and volume. After compression, the density increased from 0.57 (biocarbon powder) to 1.17 g/cm^3 (Pre-BHC), nearly doubling, which implies that more BHC samples can be processed in the same heating space and storage place, thereby improving the production efficiency. After carbonization, the density decreased from 1.17 to 1.01 g/cm^3, which indicated that a portion of the bio-oil is released during the carbonization process. However, there is no significant difference in density at different carbonization temperatures. This is because the temperature of 800 °C already exceeds the volatilization temperature of bio-oil, meaning the retention rate of bio-oil above this temperature should depend only on its infiltration rate into the biocarbon particles and its proportion within the carbon column. This is determined by the ratio of bio-oil to biocarbon during mixing as well as by the pressure applied during compression. For specific mass flow, refer to Supplementary Information given in Figs. S6 and S7. Compared to the conventional process, the method of blending bio-oil with biocarbon and compressing significantly increased the yield of HC from 20 % to 28.5 %. These enhancements optimize the HC structure and contribute to a more

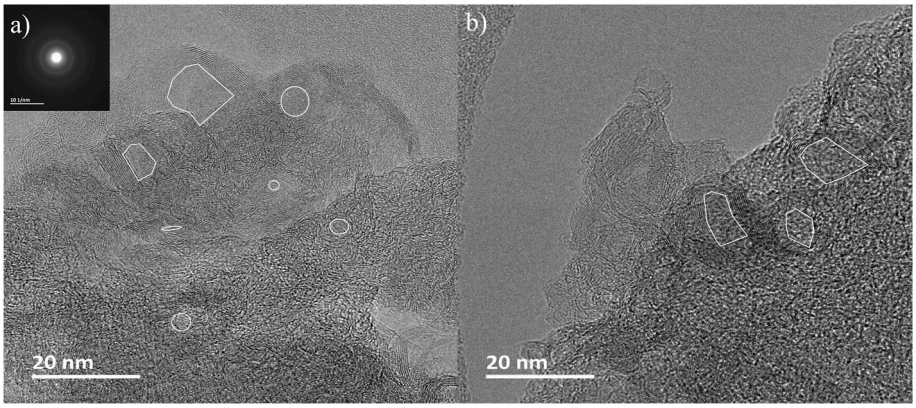

Fig. 3. High-resolution TEM and SAED images of BHC-1300.

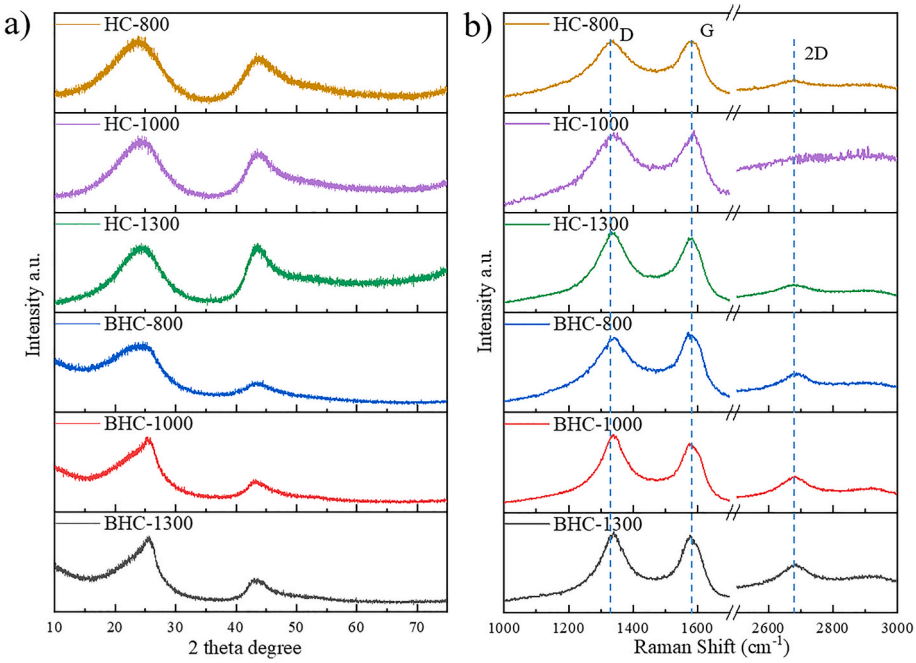

Fig. 4. a) XRD pattern of BHCs and HCs.b) Raman pattern of BHCs and HCs.

Table 2
Structure of HC and BHC samples.

Sample name	SSA m^2/g	Storage Density g/cm^3	I_D/I_G	I_{2D}/I_G	L_a nm	L_c nm	d_{002} nm
HC-800	348	–	2.17		2.88	0.89	0.38
HC-1000	58	–	2.08		3.78	1.01	0.373
HC-1300	28	–	1.86	0.23	4.32	1.07	0.371
BHC-800	330	1.01	2.2	0.35	1.95	0.95	0.376
BHC-1000	37	1.02	1.64	0.40	2.45	1.12	0.365
BHC-1300	9	1.01	1.59	0.56	3.49	1.24	0.363

sustainable and efficient production process compared to direct carbonization methods.

3.2. Electrochemical performance

The electrochemical performances of BHC and HC samples are initially assessed using SIB half-cells assembled with a mass loading of the active material ranging from 3 to 5 mg cm^{-2}. Fig. 5a shows the typical initial discharge-charge curves of three BHCs and HC-1300 electrodes in the voltage range of 0.001–2.5 V with a current density of 20 mA g^{-1}. The initial charge/discharge capacity of BHC-800, BHC-1000, BHC-1300, and HC-1300 are 204/277, 196/254, 268/298, and 244/289 mAh g^{-1}, respectively. A notable improvement in the ICE of BHC samples is observed, specifically, they increased from 73.6 % to 89.9 %. This enhancement is attributed to the reduced number of defects and open pores on the HC surface with increased carbonization temperatures [45]. The observed reduction in the reversible capacity between BHC-1000 and BHC-800 from 204 to 196 mAh g^{-1} (Fig. 5 b) can be attributed to the decreased interlayer d-spacing from 0.375 nm to approximately 0.365 nm, which hinders the intercalation of Na^+ ions [46]. This narrower d-spacing, which is particularly evident in sawdust-derived biocarbon [47], falls below the optimal Na^+ storage d-spacing range of 0.37–0.4 nm [48], leading to lower reversible capacities for BHC samples. Notably, the BHC-1300 sample exhibited higher reversible capacity and increased ICE values from 84.4 % to 89.9 % compared to the conventional process (HC-1300). This improvement is likely due to the reduction in SSA and defect of BHC-1300 after bio-oil modification. This modification decreases the electrode-electrolyte contact area, potentially minimizing the SEI formation. Additionally, the bio-oil-induced closed pore formation provides further Na^+ storage sites, which thereby enhances the reversible capacity. These findings are consistent with the results from the dQ/dV profiles (as shown in Fig. S8). During the first discharge, all four materials exhibit a broad peak around 0.5V–0.7V, which can be attributed to the formation of the SEI layer from the electrolyte [49]. As the carbonization temperature increases, the intensity of this peak decreases and gradually shifts to lower voltages, corresponding to the trend in ICE changes. Notably, BHC-1000 and BHC-1300 display additional peaks between 0.01 and 0.03V (vs Na/Na^+), which may correspond to the filling of sodium ions in closed pores and form clusters of quasi-metallic and metallic sodium [50].

Fig. 5 b presents the capacity ratios of the plateau region and the sloping region of the second discharge curves of the samples. All four materials demonstrate plateau capacity values surpassing 45 %. As the carbonization temperature rises, the capacity ratio in the plateau region notably increases and then exceeds values of 74 %. Notably, the BHC-1300 sample has a higher plateau capacity and a lower slope capacity than the HC-1300 sample.

Comparing the second discharge curve with the first discharging curve (Fig. S9), all BHC samples show a stable capacity, but the capacity of the HC-1300 sample decreased significantly from 244 to 198 mAh g^{-1}. The sloping capacities of the BHC-800, BHC-1000, BHC-1300, and HC-1300 samples are decreased to about 68, 53, 26, and 34 mAh g^{-1}, respectively, due to the irreversible formation of the SEI layer on the surface of HC samples. On the other hand, the plateau capacity of the HC-1300 sample decreased from 185 to 128 mAh g^{-1}, but the decrease in the plateau capacity of the BHC samples were minimal. This indicated that the blending of biocarbon and bio-oil and the pressing method reduced the irreversible consumption of sodium ions during charging and discharging. Among these, the BHC-1300 sample exhibited the highest plateau capacity (201 mAh g^{-1}) and plateau capacity ratio (74.8 %), which indicates that surface engineering with bio-oil could provide stable sodium-ion storage sites.

Fig. 5 c-e display the cycling performance of BHC-800, BHC-1000, and BHC-1300 electrodes at 20 mA g^{-1} for 50 cycles. All BHC electrodes

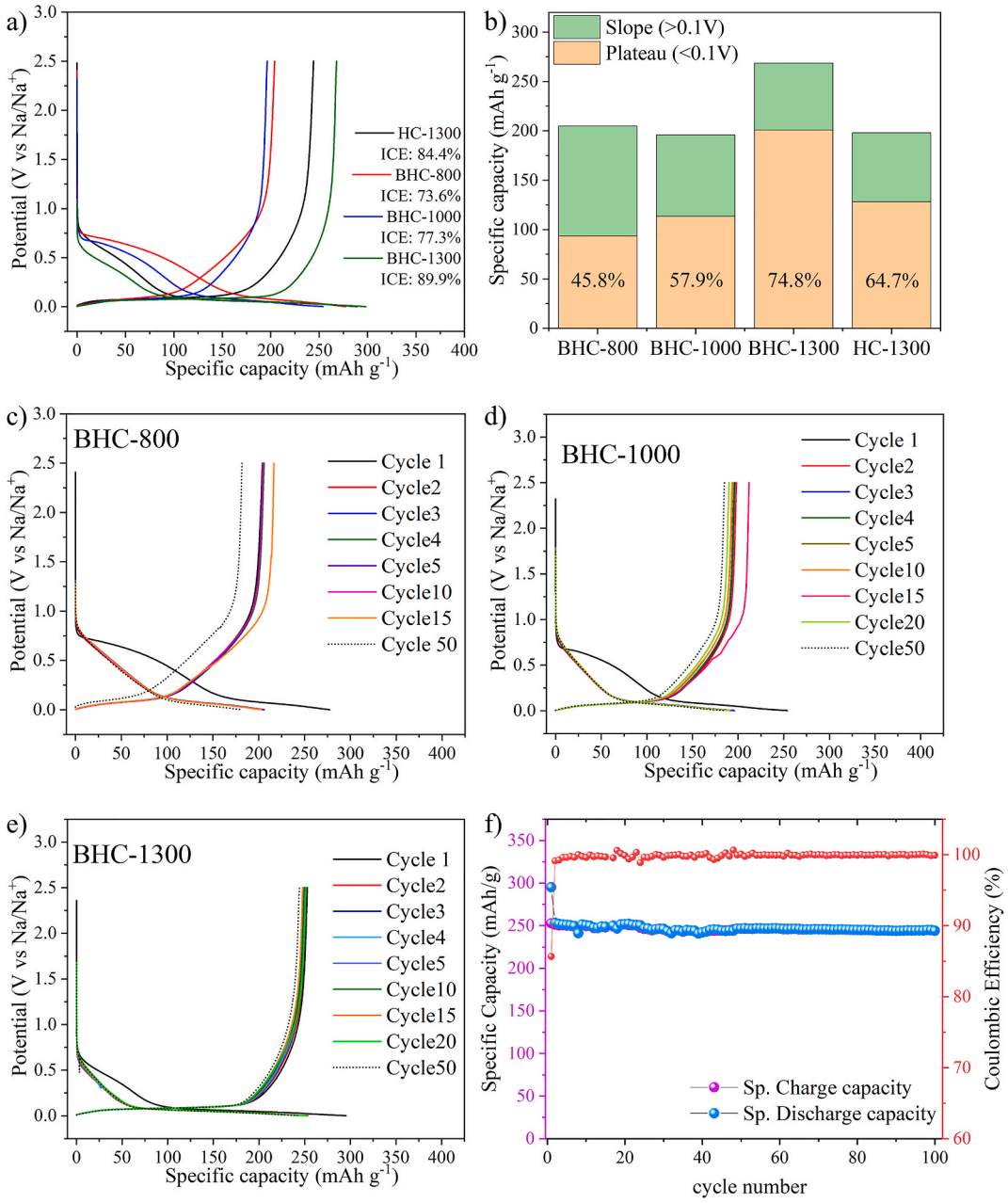

Fig. 5. a) Initial discharge/charge curves of BHCs and HC-1300 at a current rate of 20 mA g^{-1}. b) Specific capacity of BHCs and HC-1300 at plateau (<0.1 V) and slope (>0.1V) region during the second discharge curves; Discharge/charge curves of c) BHC-800, d) BHC-1000, e) BHC-1300. f) cycling performance of BHC-1300.

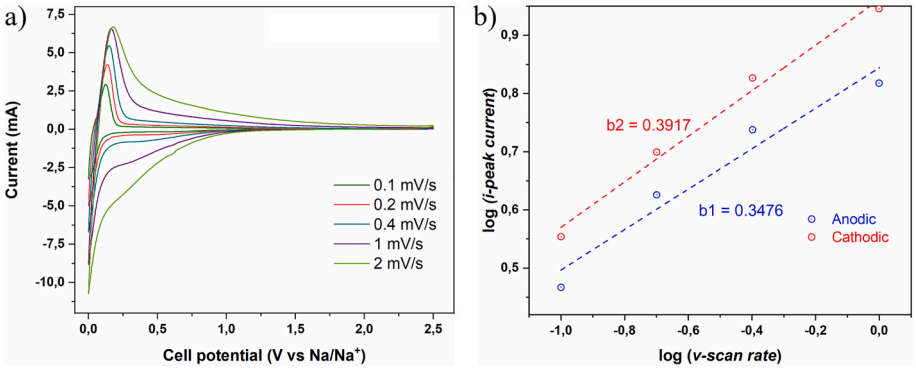

Fig. 6. a) CV curves of BHC-1300 at various scan rates from 0.1 to 2.0 mV/s. (b) The correlations of log scan rate (v) and log peak current for the anodic and cathodic peaks.

exhibit good cycle stability, with capacity retention rates above 90 % compared to the first cycle. The BHC-1300 sample, in particular, shows almost no capacity fading during cycling, maintaining a capacity retention rate of 96.5 % after 100 cycles. This further indicates that the blending of biocarbon and bio-oil and pressing methods effectively increases the stability of HC.

Cyclic voltammetry (CV) is utilized to understand the cathodic and anodic processes that occur during the charging and discharging of the electrode materials. Fig. S10 shows the CV curves of the BHC-1300 sample in the voltage range from 0.01 to 2.5 V (vs Na/Na^+) at a scan rate of 0.1 mV/s. The overlapping CV curves observed during subsequent potential sweeps implied that the anodic and cathodic processes are stable.

CV measurements were conducted at various scan rates ranging from 0.1 to 2.0 mV/s (Fig. 6a) to further investigate the Na^+ storage mechanism of the BHC-1300 anode. The low polarisation behaviour of the material during the anodic and cathodic sweeps at different scan rates was implied by a consistent shape of the CV curves. Furthermore, it was observed that the shift of the peak potentials was minimal at each of the used scan rates. Therefore, the peak potential shifts were assumed to be negligible when performing the relevant calculations mentioned below. However, when the scan rate was increased to 2.0 mV/s, it was observed that neglecting the effects of polarisation was not possible. Thus, the peak currents obtained for a 2.0 mV/s scan rate were not considered for further analysis. The power law relationship and its rearranged form mentioned below were used to analyze whether the Na^+ storage mechanism during the plateau region was (i) capacitive (a non-faradic surface-controlled process), (ii) faradaic (semi-infinite diffusion-controlled, similar to batteries) or (iii) pseudocapacitive (a faradaic charge-transfer process controlled by the surface characteristics) [51,52].

$$i = av^b$$

$$\log(i) = b \times \log(v) + \log(c)$$

In the above equations, i is the measured peak current at a particular scan rate v at a specific potential (e.g., the potential where the peak current is observed), whereas a and b correspond to a constant and the power law exponent, respectively. The gradient of the plot between log (i) and log(v) corresponds to the b value. Based on the value of b, the Na^+ storage mechanism can be determined to be either faradaic, capacitive, or pseudocapacitive. If the value of b is 0.5 (b = 0.5), a faradic-diffusion-controlled process becomes dominant, whereas when the value of b is 01 (b = 1), a capacitive charge storage mechanism becomes dominant [53]. It was observed that the b values of both the anodic and cathodic processes of BHC-1300 at scan rates from 0.1 to 1.0 mV/s were close to a value of 0.5 (b1 = 0.3476, b2 = 0.3917). This implied that the Na + storage/removal mechanism from the material was dominated by diffusion (in the plateau region).

3.3. Life cycle assessment

As stated before, LCA is performed to provide a deeper understanding of the two different synthetic processes (HC-1300 and BHC-1300) of sawdust-derived HCs and compare their environmental performance. It should be noted that the impact of the use and the end-of-life phases is out of the focus of this study. Due to data availability and the focus of this study in comparing different synthetic process pathways of HC production, a cradle-to-gate framework is applied for this LCA study. However, it is highly important to include these phases in future assessments when further data is available, as these phases can have a high impact on the overall environmental performance of sodium-ion batteries [54]. In addition, the modeling is conducted based on the primary data collected directly from the laboratory. Therefore, substantially higher environmental impacts are expected with respect to the industrial-scale LCA study of HC production [35]. Accordingly, the sustainability of the HC synthesis can be improved via a more sustainable furnace to enable large-scale production with higher efficiency and throughput. Additionally, further optimization options, such as obtaining a cleaner energy and supply chain should be explored.

The LCA results to produce 1 kg HC material are depicted in Fig. 7a (more details regarding inventory data and all calculated environmental impacts can be found in Tables S4–S6 and Fig. S11). Compared to conventional production methods (HC-1300 scenarios), the blending of bio-oil and pressing method (BHC-1300 scenario) reduces the GWP value in HC production by 19.9 %. This reduction mainly stems from the higher carbon yield and efficiency in the carbonization process, which decreases the electricity consumption for the production process. As result, emissions stemming from pyrolysis gas during the production of 1 kg HC are reduced. Other environmental impacts such as the RDP, WRP, AP, PM, and HT have decreased by nearly 24 %. These reductions in impact factors can primarily be attributed to the lower electricity inputs during the BHC production process.

Fig. 7b shows the main contributors to greenhouse gas emissions in HC production. Among these, emissions from the pyrolysis process account for 49.48 % of the total emissions in conventional production with the base case (conventional production process HC-1300, under the Swedish electricity mix 2018). The BHC-1300 case shows a substantial reduction in GWP during its production, marked by a decline in carbon emissions from 25.89 to 20.53 kg CO_2-eq./kg_{HC}. This improvement can primarily be attributed to two key factors. Firstly, the introduction of bio-oil enhances the carbon yield during the devolatilization process, as illustrated in Figs. S5 and S6. This is because bio-oil acts as a carbon-rich precursor, which improves the formation of HC upon carbonization. This, in turn, enhances the yield from biomass to HC from 19.33 % to 26.9 %. This means that the amount of biomass required to produce HC has decreased from 5.17 to 3.72 kg/kg_{HC}, reducing the amount of biomass needed for the pyrolysis process. Consequently, emissions from the pyrolysis process can be reduced by 29.8 %. Secondly, the mixture of biocarbon and bio-oil, when compressed, forms columns of high density. This allows for a greater quantity to be accommodated within the furnace. This results in a lower energy consumption per unit and simplifies both the transport and storage processes. After compression, the density of biocarbon increased from 0.58 g/cm^3 to 1.17 g/cm^3. This means that nearly double the amount of biocarbon can be processed in the same furnace. Thus, the energy consumption per unit, as shown in Fig. 7c, for the devolatilization process is reduced from 76.89 kWh/kg_{HC} to 59.19 kWh/kg_{HC}. Furthermore, for the carbonization process, it is decreased from 108.58 kWh/kg_{HC} to 68.25 kWh/kg_{HC} (based on laboratory equipment). Additionally, the compressed biocarbon blocks, when compared to powder, exhibit superior thermal conductivities. This characteristic potentially enables a uniform quality and further reductions in the energy demand for thermal processing.

Since HC production is primarily reliant on electricity consumption, a LCA focusing on alternative power sources and supply chains for HC production is conducted to evaluate the environmental impact in different regions available in Eocinvent 3.8. As seen in Fig. 7d, the source of electricity plays a significant role in the environmental burden related to the HC production. For instance, Sweden, which primarily uses sustainable energy sources (40 % hydroelectricity, 29 % nuclear and 20 % wind power [55]), exhibits the lowest greenhouse gas emissions of 18.07 kg CO_2-eq. The use of nuclear power has contributed to the relative high ionizing radiation potential of Sweden's electricity supply. China, with over 60 % ratios on coal in 2023 [56], has notably high impacts, amounting to 312.73 kg CO_2-eq./kg_{HC}. German with almost 50 % renewables (mainly wind, PV, and biomass) but still over 20 % fossil-based electricity (lignite and hard coal) in 2023 [57] lies between these two countries with 160 kg CO_2-eq./kg_{HC}. However, upon adopting the method of mixing and pressing with bio-oil, both countries witnessed significant reductions in carbon emissions. Specifically, using German electricity, this method reduces emissions by 37.85 kg CO_2-eq./kg_{HC}. Furthermore, when relying on Chinese electricity, there's

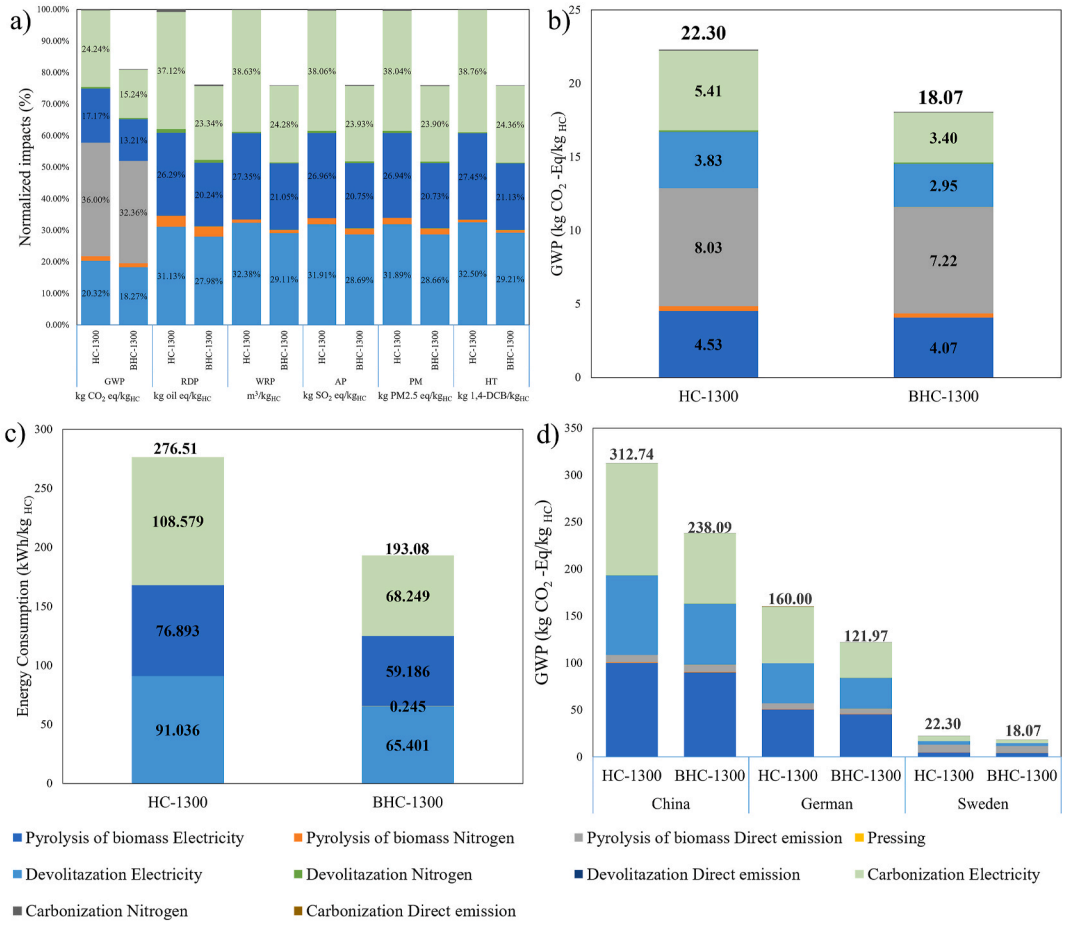

Fig. 7. LCA result of a) Environment impact of different categories of HC-1300 and BHC-1300; b) GWP of HC-1300 and BHC-1300; c) Energy consumption of HC-1300 and BHC-1300; d) GWP of BHC-1300 with electricity mix and supply chain of different countries.

a reduction of 74.64 kg CO_2-eq./kg_{HC}. Additionally, with the global energy shift towards cleaner sources, using 100 % renewable energy sources such as wind or solar power for HC production is a future trend that could significantly cut emissions. Ignoring the synthetic gas emissions from pyrolysis and using it as an energy product, the greenhouse gas emissions for producing 1 kg of HC using wind power could be reduced to 7.73 kg CO_2-eq./kg_{HC} using traditional production methods. This figure could further decrease to 5.89 kg CO_2-eq./kg_{HC} when bio-oil blending is employed as shown in Fig. S12. Again, stressing that this result is based on laboratory scale results. Therefore, a further reduction of environmental impact can be expected when production is scaled up in the future and reaching higher efficiency.

Overall, the method of blending and pressing using bio-oil notably reduces the environmental impact associated with a HC production by boosting its yield and optimizing its processing volume.

4. Discussion

Fig. S13 illustrates the working mechanism of bio-oil combined with high-pressure compression. Bio-oil functions as a surface engineering agent, analogous to pitch or benzene used in blending and CVD processes. High-pressure compression further enhances bio-oil infiltration into the open pores of biocarbon. This compression not only promotes deeper penetration but also prevents the free escape of volatile components during carbonization, thereby extending their retention within the carbon block [58]. This prolonged retention significantly facilitates carbon formation via the decomposition of these volatiles [59]. Consequently, after the carbonization process, carbon layers are formed, leading to the reduce of open pores and the increase of ICE value from 84 % (HC-1300) to around 90 % (BHC-1300).

Compared with the conventional approach followed by a blending or a CVD approach (Table S1), our process is more streamlined and is emancipated from the dependence on fossil fuel based surface engineering agent such as pitch and benzene. Moreover, because bio-oil is derived from the same production process as biocarbon, its use as both a binder and a surface engineering agent not only improves the HC yield but also enhances the storage density of HC, thereby increasing the processing volume. This, in turn, reduces the GWP and contributes to a more sustainable HC production process.

5. Conclusion

The present study proposes an innovative bio-oil surface engineering process to produce HC anode material from sawdust-based biomass, which involves mixing bio-oil with biocarbon and subsequently compressing the mixture to form HC columns. Specifically, the physical and electrochemical performance of the resulting HC product is investigated. In addition, a cradle-to-gate LCA study is conducted to identify environmental benefits and burdens for the proposed HC production process. The promising production process significantly reduces the SSA of HC, modifies surface defects, increases the closed pore volume, and thus enhances the ICE of HC. The optimized sample, BHC-1300, achieved a promising ICE value of 89.9 % and a reversible capacity of 268 mAh g^{-1}. In addition, the proposed production process increased the yield of HC by 39 % and enhanced the processing volume in the heating furnace, which significantly reduced the energy demand. As a result, the overall

greenhouse gas emission can be reduced to as low as 18.07 kg CO_2-eq./kg_{HC}, which corresponds to a 20 % reduction. This research offers an easy, sustainable, practical, and cost-competitive new surface engineering pretreatment process for HC.

CRediT authorship contribution statement

Yanghao Jin: Writing – review & editing, Writing – original draft, Visualization, Validation, Methodology, Investigation, Data curation, Conceptualization. **Huiting Liu:** Writing – review & editing, Writing – original draft, Validation, Software, Methodology, Formal analysis, Data curation, Conceptualization. **Hanmin Yang:** Writing – review & editing, Validation, Supervision, Formal analysis, Conceptualization. **Dumindu Pasan Siriwardena Thanaweera Achchige:** Writing – review & editing, Validation, Methodology, Investigation, Formal analysis, Data curation. **Yaprak Subasi:** Writing – review & editing, Validation, Formal analysis, Data curation. **Ritambhara Gond:** Writing – review & editing, Validation, Formal analysis, Data curation. **Yazhe Wang:** Visualization, Validation. **Habtom Desta Asfaw:** Writing – review & editing, Validation, Supervision. **Shiwei Chen:** Writing – review & editing, Data curation. **Ziyi Shi:** Writing – review & editing, Visualization, Validation, Supervision, Methodology, Formal analysis, Conceptualization. **Tong Han:** Writing – review & editing, Visualization, Validation, Supervision, Methodology, Formal analysis, Data curation. **Manuel Baumann:** Writing – review & editing, Supervision, Resources. **Niklas von der Assen:** Writing – review & editing, Supervision, Resources. **Marcel Weil:** Writing – review & editing, Supervision, Resources, Funding acquisition. **Reza Younesi:** Writing – review & editing, Supervision, Resources, Project administration, Funding acquisition. **Pär G. Jönsson:** Writing – review & editing, Supervision, Resources. **Weihong Yang:** Writing – review & editing, Supervision, Resources, Project administration, Funding acquisition.

Declaration of competing interest

The authors declare the following financial interests/personal relationships which may be considered as potential competing interests: Yanghao Jin, Dumindu Pasan Siriwardena Thanaweera Achchige reports financial support was provided by Sweden's Innovation Agency. Reza Younesi reports financial support was provided by Swedish Energy Agency. Huiting Liu, Marcel Weil, Manuel Baumann reports financial support was provided by German Research Foundation. Yanghao Jin, Tong Han, Weihong Yang has patent #2024100436391 pending to licensee. If there are other authors, they declare that they have no known competing financial interests or personal relationships that could have appeared to influence the work reported in this paper.

Acknowledgement

The supply of raw materials for the experiments by Envigas is greatly appreciated. The TEM test support by Cheuk-Wai Tai from ARTEMI is appreciated. The financial support by VINNOVA, Sweden via the project number 2021–03735 is highly appreciated. This work contributes also to the research performed at CELEST (Center for Electrochemical Energy Storage Ulm-Karlsruhe). H. Liu, M. Weil, M. Baumann acknowledge the financial support by the German Research Foundation, Germany (DFG, Germany) under Project ID 390874152 (POLiS Cluster of Excellence, EXC 2154).

Appendix A. Supplementary data

Supplementary data to this article can be found online at https://doi.org/10.1016/j.jpowsour.2025.236824.

Data availability

The data that has been used is confidential.

References

[1] K. Sada, J. Darga, A. Manthiram, Challenges and prospects of sodium-ion and potassium-ion batteries for mass production, Adv. Energy Mater. 13 (2023) 2302321, https://doi.org/10.1002/aenm.202302321.
[2] P. Yadav, V. Shelke, A. Patrike, M. Shelke, Sodium-based batteries: development, commercialization journey and new emerging chemistries, Oxford Open Materials Science 3 (2023) itac019, https://doi.org/10.1093/oxfmat/itac019.
[3] A. Buckel, C.A. Hall, L.A. Ma, L.S. Colbin, H. Eriksson, R. Mogensen, R. Younesi, Importance of first cycle conditions on the electrochemical performance of hard carbon and prussian white based sodium-ion batteries using fire resistant, fluorine-free electrolyte, Batteries & Supercaps (2023) e202300533, https://doi.org/10.1002/batt.202300533.
[4] X. Dou, I. Hasa, D. Saurel, C. Vaalma, L. Wu, D. Buchholz, D. Bresser, S. Komaba, S. Passerini, Hard carbons for sodium-ion batteries: structure, analysis, sustainability, and electrochemistry, Mater. Today 23 (2019) 87–104, https://doi.org/10.1016/j.mattod.2018.12.040.
[5] R. Li, B. Yang, A. Hu, B. Zhou, M. Liu, L. Yang, Z. Yan, Y. Fan, Y. Pan, J. Chen, Heteroatom screening and microcrystal regulation of coal-derived hard carbon promises high-performance sodium-ion batteries, Carbon 215 (2023) 118489, https://doi.org/10.1016/j.carbon.2023.118489.
[6] M.K. Le, T.N. Tran, T.K.T. Huynh, D.T. Vo, M.L.P. Le, Development of Vang Danh anthracite as a cost-effective anode for sodium-ion batteries through a heat-treatment process, RSC Adv. 12 (2022) 29900–29907, https://doi.org/10.1039/D2RA05514G.
[7] C.d.M.S. Rios, V. Simone, L. Simonin, S. Martinet, C. Dupont, Biochars from various biomass types as precursors for hard carbon anodes in sodium-ion batteries, Biomass Bioenergy 117 (2018) 32–37, https://doi.org/10.1016/j.biombioe.2018.07.001.
[8] H. Liu, M. Baumann, H. Moon, X. Zhang, X. Dou, M. Zarrabeitia, E. Crenna, R. Hischier, S. Passerini, N. von der Assen, Life cycle assessment of bio-based hard carbon for sodium-ion batteries across different production scales, Chem. Eng. J. (2024) 153410.
[9] W. Shao, H. Shi, X. Jian, Z.-S. Wu, F. Hu, Hard-carbon anodes for sodium-ion batteries: recent status and challenging perspectives, Advanced Energy and Sustainability Research 3 (2022) 2200009, https://doi.org/10.1002/aesr.202200009.
[10] D. Alvira, D. Antorán, J.J. Manyà, Plant-derived hard carbon as anode for sodium-ion batteries: a comprehensive review to guide interdisciplinary research, Chem. Eng. J. 447 (2022) 137468, https://doi.org/10.1016/j.cej.2022.137468.
[11] M. Thompson, Q. Xia, Z. Hu, X.S. Zhao, A review on biomass-derived hard carbon materials for sodium-ion batteries, Materials Advances 2 (2021) 5881–5905, https://doi.org/10.1039/D1MA00315A.
[12] H. Liu, M. Baumann, X. Dou, J. Klemens, L. Schneider, A.-K. Wurba, M. Häringer, P. Scharfer, H. Ehrenberg, W. Schabel, Tracing the technology development and trends of hard carbon anode materials-A market and patent analysis, J. Energy Storage 56 (2022) 105964, https://doi.org/10.1016/j.est.2022.105964.
[13] M.R.B. Domalanta, M.T. Castro, J.A.D. Del Rosario, J.D. Ocon, Cost analysis of a sodium-ion battery pack for energy and power applications using combined multi-physics and techno-economic modeling, Chemical Engineering Transactions 94 (2022) 139–144, https://doi.org/10.3303/CET2294023.
[14] H. Moon, A. Innocenti, H. Liu, H. Zhang, M. Weil, M. Zarrabeitia, S. Passerini, Bio-waste-derived hard carbon anodes through a sustainable and cost-effective synthesis process for sodium-ion batteries, ChemSusChem 16 (2023) e202201713, https://doi.org/10.1002/cssc.202201713.
[15] F. Trotta, G.J. Wang, Z. Guo, Z. Xu, M. Crespo Ribadeneyra, H. Au, J.S. Edge, M. M. Titirici, L. Lander, A comparative techno-economic and lifecycle analysis of biomass-derived anode materials for lithium-and sodium-ion batteries, Advanced Sustainable Systems 6 (2022) 2200047, https://doi.org/10.1002/adsu.202200047.
[16] S. Kulkarni, T.-Y. Huang, B.P. Thapaliya, H. Luo, S. Dai, F. Zhao, Prospective life cycle assessment of synthetic graphite manufactured via electrochemical graphitization, ACS Sustain. Chem. Eng. 10 (2022) 13607–13618, https://doi.org/10.1021/acssuschemeng.2c02937.
[17] D. Surovtseva, E. Crossin, R. Pell, L. Stamford, Toward a life cycle inventory for graphite production, J. Ind. Ecol. 26 (2022) 964–979, https://doi.org/10.1111/jiec.13234.
[18] G. Bhutada, Battery down the cost of an EV battery cell. https://www.visualcapitalist.com/breaking-down-the-cost-of-an-ev-battery-cell/,2022. (Accessed 3 October 2023).
[19] M. Zhang, Y. Li, F. Wu, Y. Bai, C. Wu, Boost sodium-ion batteries to commercialization: strategies to enhance initial Coulombic efficiency of hard carbon anode, Nano Energy 82 (2021) 105738, https://doi.org/10.1016/j.nanoen.2020.105738.
[20] G. Jiang, L. Liu, J. Xiong, Y. Luo, L. Cai, Y. Qian, H. Wang, L. Mu, X. Feng, X. Lu, Advanced material-oriented biomass precise reconstruction: a review on porous carbon with inherited natural structure and created artificial structure by post-treatment, Macromol. Biosci. 22 (2022) 2100479, https://doi.org/10.1002/mabi.202100479.

[21] Y. Yang, C. Wu, X.X. He, J. Zhao, Z. Yang, L. Li, X. Wu, L. Li, S.L. Chou, Boosting the development of hard carbon for sodium-ion batteries: strategies to optimize the initial coulombic efficiency, Adv. Funct. Mater. 34 (2024) 2302277.
[22] Y. Wan, Y. Liu, D. Chao, W. Li, D. Zhao, Recent advances in hard carbon anodes with high initial Coulombic efficiency for sodium-ion batteries, Nano Materials Science (2022), https://doi.org/10.1016/j.nanoms.2022.02.001.
[23] Y. Li, S. Xu, X. Wu, J. Yu, Y. Wang, Y.-S. Hu, H. Li, L. Chen, X. Huang, Amorphous monodispersed hard carbon micro-spherules derived from biomass as a high performance negative electrode material for sodium-ion batteries, J. Mater. Chem. A 3 (2015) 71–77, https://doi.org/10.1039/C4TA05451B.
[24] Y. Zhang, N. Zhang, W. Chen, Z. Rao, J. Wu, L. Xue, W. Zhang, Effect of vapor carbon coating on the surface structure and sodium storage performance of hard carbon spheres, Energy Technol. 7 (2019) 1900779, https://doi.org/10.1002/ente.201900779.
[25] H. Chen, N. Sun, Y. Wang, R.A. Soomro, B. Xu, One stone two birds: pitch assisted microcrystalline regulation and defect engineering in coal-based carbon anodes for sodium-ion batteries, Energy Storage Mater. 56 (2023) 532–541, https://doi.org/10.1016/j.ensm.2023.01.042.
[26] X. Zhang, W. Chen, J. Peng, Y. Guo, L. Cheng, N. Chen, R. Du, Y. Huang, L. Xue, W. Zhang, Pore structure modification of pitch-derived hard carbon for enhanced pore filling sodium storage, Energy Technol. 10 (2022) 2200612.
[27] X. Chen, N. Sawut, K. Chen, H. Li, J. Zhang, Z. Wang, M. Yang, G. Tang, X. Ai, H. Yang, Filling carbon: a microstructure-engineered hard carbon for efficient alkali metal ion storage, Energy Environ. Sci. (2023), https://doi.org/10.1039/D3EE01154B.
[28] E. Union, European union brussels, Belgium, http://data.europa.eu/eli/reg/2023/1542/oj, 2023.
[29] A. Ochoa, J. Bilbao, A.G. Gayubo, P. Castaño, Coke formation and deactivation during catalytic reforming of biomass and waste pyrolysis products: a review, Renew. Sustain. Energy Rev. 119 (2020) 109600, https://doi.org/10.1016/j.rser.2019.109600.
[30] S. Xiu, A. Shahbazi, Bio-oil production and upgrading research: a review, Renew. Sustain. Energy Rev. 16 (2012) 4406–4414.
[31] X. Hu, K. Nango, L. Bao, T. Li, M.M. Hasan, C.-Z. Li, High yields of solid carbonaceous materials from biomass, Green Chem. 21 (2019) 1128–1140, https://doi.org/10.1039/C8GC03153C.
[32] N. Iwashita, C.R. Park, H. Fujimoto, M. Shiraishi, M. Inagaki, Specification for a standard procedure of X-ray diffraction measurements on carbon materials, Carbon 42 (2004) 701–714, https://doi.org/10.1016/j.carbon.2004.02.008.
[33] T. Qiu, J.-G. Yang, X.-J. Bai, Y.-L. Wang, The preparation of synthetic graphite materials with hierarchical pores from lignite by one-step impregnation and their characterization as dye absorbents, RSC Adv. 9 (2019) 12737–12746, https://doi.org/10.1039/C9RA00343F.
[34] B. Xiao, T. Rojo, X. Li, Hard carbon as sodium-ion battery anodes: progress and challenges, ChemSusChem 12 (2019) 133–144, https://doi.org/10.1002/cssc.201801879.
[35] M. Erakca, S.P. Bautista, S. Moghaddas, M. Baumann, W. Bauer, L. Leuthner, M. Weil, Closing gaps in LCA of lithium-ion batteries: LCA of lab-scale cell production with new primary data, J. Clean. Prod. 384 (2023) 135510, https://doi.org/10.1016/j.jclepro.2022.135510.
[36] J.F. Peters, M. Baumann, B. Zimmermann, J. Braun, M. Weil, The environmental impact of Li-Ion batteries and the role of key parameters–A review, Renew. Sustain. Energy Rev. 67 (2017) 491–506, https://doi.org/10.1016/j.rser.2016.08.039.
[37] A. Gomez-Martin, J. Martinez-Fernandez, M. Ruttert, M. Winter, T. Placke, J. Ramirez-Rico, Correlation of structure and performance of hard carbons as anodes for sodium ion batteries, Chem. Mater. 31 (2019) 7288–7299.
[38] B.-L. Xing, H. Guo, L.-J. Chen, Z.-F. Chen, C.-X. Zhang, G.-X. Huang, W. Xie, J.-L. Yu, Lignite-derived high surface area mesoporous activated carbons for electrochemical capacitors, Fuel Process. Technol. 138 (2015) 734–742, https://doi.org/10.1016/j.fuproc.2015.07.017.
[39] Y. Chu, J. Zhang, Y. Zhang, Q. Li, Y. Jia, X. Dong, J. Xiao, Y. Tao, Q.H. Yang, Reconfiguring hard carbons with emerging sodium-ion batteries: a perspective, Adv. Mater. (2023) 2212186.
[40] X. Wu, X. Yang, F. Zhang, L. Cai, L. Zhang, Z. Wen, Carbon-coated isotropic natural graphite spheres as anode material for lithium-ion batteries, Ceram. Int. 43 (2017) 9458–9464, https://doi.org/10.1016/j.ceramint.2017.04.123.
[41] Y. Liu, Y.X. Lu, Y.S. Xu, Q.S. Meng, J.C. Gao, Y.G. Sun, Y.S. Hu, B.B. Chang, C. T. Liu, A.M. Cao, Pitch-derived soft carbon as stable anode material for potassium ion batteries, Adv. Mater. 32 (2020) 2000505, https://doi.org/10.1002/adma.202000505.
[42] X.-X. He, J.-H. Zhao, W.-H. Lai, R. Li, Z. Yang, C.-m. Xu, Y. Dai, Y. Gao, X.-H. Liu, L. Li, Soft-carbon-coated, free-standing, low-defect, hard-carbon anode to achieve a 94% initial coulombic efficiency for sodium-ion batteries, ACS Appl. Mater. Interfaces 13 (2021) 44358–44368.
[43] X. Li, J. Sun, W. Zhao, Y. Lai, X. Yu, Y. Liu, Intergrowth of graphite-like crystals in hard carbon for highly reversible Na-ion storage, Adv. Funct. Mater. 32 (2022) 2106980, https://doi.org/10.1002/adfm.202106980.
[44] Y. Li, Y. Lu, Q. Meng, A.C. Jensen, Q. Zhang, Q. Zhang, Y. Tong, Y. Qi, L. Gu, M. M. Titirici, Regulating pore structure of hierarchical porous waste cork-derived hard carbon anode for enhanced Na storage performance, Adv. Energy Mater. 9 (2019) 1902852, https://doi.org/10.1002/aenm.201902852.
[45] L. Kitsu Iglesias, E.N. Antonio, T.D. Martinez, L. Zhang, Z. Zhuo, S.J. Weigand, J. Guo, M.F. Toney, Revealing the sodium storage mechanisms in hard carbon pores, Adv. Energy Mater. 13 (2023) 2302171, https://doi.org/10.1002/aenm.202302171.
[46] S. Alvin, H.S. Cahyadi, J. Hwang, W. Chang, S.K. Kwak, J. Kim, Revealing the intercalation mechanisms of lithium, sodium, and potassium in hard carbon, Adv. Energy Mater. 10 (2020) 2000283, https://doi.org/10.1002/aenm.202000283.
[47] Z.-T. Liu, T.-H. Hsieh, C.-W. Huang, M.-L. Lee, W.-R. Liu, Temperature effects on hard carbon derived from sawdust as anode materials for sodium ion batteries, J. Taiwan Inst. Chem. Eng. 154 (2024) 104889, https://doi.org/10.1016/j.jtice.2023.104889.
[48] Z. Tian, Y. Zhang, J. Zhu, Q. Li, T. Liu, M. Antonietti, A reanalysis of the diverse sodium species in carbon anodes for sodium ion batteries: a thermodynamic view, Adv. Energy Mater. 11 (2021) 2102489, https://doi.org/10.1002/aenm.202102489.
[49] A. Kumar Nagmani, S. Puravankara, Optimizing ultramicroporous hard carbon spheres in carbonate ester-based electrolytes for enhanced sodium storage in half-/full-cell sodium-ion batteries, Battery Energy 1 (2022) 20220007, https://doi.org/10.1002/bte2.20220007.
[50] V. Surendran, R.K. Hema, M.S.O. Hassan, V. Vijayan, M.M. Shaijumon, Open or closed? Elucidating the correlation between micropore nature and sodium storage mechanisms in hard carbon, Batteries & Supercaps 5 (2022) e202200316, https://doi.org/10.1002/batt.202200316.
[51] K. Wang, M. Li, Z. Zhu, W. Ai, H. Wu, B. Wang, P. He, D. Xie, J. Wu, W. Huang, Hard carbon with embedded graphitic nanofibers for fast-charge sodium-ion batteries, Nano Energy 124 (2024) 109459.
[52] J.F. Fernando, D.P. Siriwardena, K.L. Firestein, C. Zhang, J.E. von Treifeldt, C.-E. M. Lewis, T. Wang, D.P. Dubal, D.V. Golberg, Enriched pseudocapacitive lithium storage in electrochemically activated carbonaceous vanadium (iv, v) oxide hydrate, J. Mater. Chem. A 8 (2020) 13183–13196.
[53] S. Fleischmann, J.B. Mitchell, R. Wang, C. Zhan, D.-e. Jiang, V. Presser, V. Augustyn, Pseudocapacitance: from fundamental understanding to high power energy storage materials, Chem. Rev. 120 (2020) 6738–6782.
[54] J.F. Peters, M. Baumann, J.R. Binder, M. Weil, On the environmental competitiveness of sodium-ion batteries under a full life cycle perspective–a cell-chemistry specific modelling approach, Sustain. Energy Fuels 5 (2021) 6414–6429, https://doi.org/10.1039/D1SE01292D.
[55] IEA, Electricity generation, Sweden, https://www.iea.org/countries/sweden/energy-mix,2023. (Accessed 25 January 2025).
[56] IEA, Electricity generation, China, https://www.iea.org/countries/china,2023. (Accessed 8 March 2024).
[57] IEA, Electricity generation, German, https://www.iea.org/countries/germany/electricity,2025, 2023. (Accessed 25 January 2025).
[58] Y. Chen, S.S.A. Syed-Hassan, Q. Li, Z. Deng, X. Hu, J. Xu, L. Jiang, S. Su, S. Hu, Y. Wang, Effects of temperature and aspect ratio on heterogeneity of the biochar from pyrolysis of biomass pellet, Fuel Process. Technol. 235 (2022) 107366.
[59] S. Zhang, Z. Min, H.-L. Tay, M. Asadullah, C.-Z. Li, Effects of volatile–char interactions on the evolution of char structure during the gasification of Victorian brown coal in steam, Fuel 90 (2011) 1529–1535.